



Ideal MHD stability calculations for compact stellarators

R. Sanchez^{a,*}, M.Yu. Isaev^b, S.P. Hirshman^c, W.A. Cooper^d, G.Y. Fu^e, J.A. Jimenez^f,
L.P. Ku^e, M.I. Mikhailov^b, D.A. Monticello^e, A.H. Reiman^e, A.A. Subbotin^b

^a *Departamento de Física, Universidad Carlos III de Madrid, Madrid, Spain*

^b *Nuclear Fusion Institute, RRC “Kurchatov Institute”, Moscow, Russia*

^c *Oak Ridge National Laboratory, Oak Ridge, TN, USA*

^d *Centre de Recherches en Physique des Plasmas, Association Euratom-Suisse, Ecole Polytechnique Federale de Lausanne, CRPP-PPB, Lausanne, Switzerland*

^e *Princeton Plasma Physics Laboratory, Princeton, NJ, USA*

^f *Asociación Euratom-CIEMAT, Madrid, Spain*

Received 9 March 2001; received in revised form 14 May 2001; accepted 24 May 2001

Abstract

Stability results for high- n ideal local pressure-driven instabilities (ballooning and interchange modes) are calculated from the COBRA and TERPSICHORE codes and compared for several low aspect ratio stellarators. Such a comparison is important because of the predominant roles that these codes are playing in the design of compact stellarators at several laboratories around the world. The code development required to reach the levels of convergence and accuracy needed for reliable operation at low aspect ratios is also described. © 2001 Elsevier Science B.V. All rights reserved.

PACS: 02.60.Lj; 52.35.Py; 52.55.Mc; 52.55.Kj

Keywords: Stellarators; Low aspect ratio; Magnetohydrodynamics; Ideal pressure-driven instabilities; Interchange and ballooning modes; Magnetic coordinates

1. Introduction

The stellarator concept was first proposed many years ago [1]. However, renewed interest in this concept as a possible means to a future fusion reactor has increased during the last decade due to at least two factors:

(1) the possibility of reducing neoclassical losses to levels comparable to equivalent tokamaks by using magnetic fields exhibiting so-called quasi-symmetries [2] and

(2) the increasing availability of faster and more sophisticated numerical tools that can be used within a feasible numerical optimization scheme [3,4] to identify those quasi-symmetric 3D configurations simultaneously exhibiting other convenient physical properties (including but not limited to equilibrium, stability, bootstrap current, and coil feasibility).

Compact stellarators have received a lot of attention due to the smaller size (and cost) of the reactors that might originate from them. These stellarators have aspect ratios $A < 4$, with $A \equiv R_0/a$ the ratio of the major to the plasma radius. In comparison,

* Corresponding author.

E-mail address: rsanchez@fis.uc3m.es (R. Sanchez).

the state-of-the-art stellarators in the world, the Wendelstein 7-X stellarator in Germany [5] and the Large Helical Device (LHD) in Japan [6] have much larger aspect ratios, $A \sim 12$ and $A \sim 8$, respectively. Several laboratories throughout the world are currently pursuing compact stellarators: quasi-axisymmetric stellarators (QAS) are being designed at both the Princeton Plasma Physics Laboratory (the National Compact Stellarator Experiment or NCSX) [7,8] and at the National Institute for Fusion Science in Japan (the CHS-qa, a quasi-axisymmetric variation of the Compact Helical System (CHS) already in operation) [9]); the Oak Ridge National Laboratory has instead developed a related concept based on quasi-omnigenity [10], and is designing a quasi-omnigenous compact stellarator (QOS, recently renamed QPS since further optimization has made the design become quasi-poloidally symmetric) [11,12].

The search for attractive compact configurations must be carried out numerically using fully three-dimensional (3D) codes, since the conditions that validate the use of analytical approximations [13] or toroidally-averaged 2D codes [14], i.e. $A \gg 1$ and $\tau/N \ll 1$ (N is the periodicity and τ the rotational transform), are strongly violated. In addition to the more extreme geometry compared with larger aspect ratio stellarators, the nature of the optimization method used in the design [4] also makes these calculations even more demanding in terms of convergence and accuracy, especially with respect to stability: an inaccurate assessment can point the optimizer towards the wrong (and more unstable) path in parameter space and render the optimization meaningless!

This situation has stimulated the development of many existing codes and the creation of some new ones [4,7,8,12], not limited to the stability codes we will focus on in this paper. As part of this effort, a new ideal ballooning code, COBRA [15,16], has been created which is sufficiently fast and numerically reliable to be included into the optimization process (see Section 3). It has been specifically developed to converge well at low aspect ratios and is able to avoid many of the convergence and accuracy problems that affect the other widely used stellarator stability codes. These problems manifest themselves in several ways: (1) as a lack of convergence and/or accuracy of the equilibrium solution, usually obtained by the VMEC equilibrium solver [17] or/and (2) a lack

of convergence and/or accuracy in the conversion of the VMEC solution into the coordinate system used by the stability code, usually that introduced by Boozer [18] (for instance, this is the case of the TERPSICHORE [19], CAS3D [20] or JMC [21] codes). COBRA is only affected by the first problem, since it uses the same magnetic coordinates as VMEC. But the recent improvements of the VMEC code, briefly reviewed in Section 2, have enhanced its reliability even further for use within the optimization process.

COBRA's performance is however a consequence of its high degree of specialization: its domain of applicability is limited to high- n local pressure-driven modes, namely ballooning and interchange modes. These are usually the limiting instabilities for nearly currentless configurations (this is the case of most QOS designs). But NCSX configurations usually have toroidal currents of hundreds of kA flowing in the plasma, which can drive current-driven modes that set the critical $\langle \beta \rangle$ in some cases. Some control of the kink instability during the optimization process is accomplished by using an approximate analytic criterion [22], but quasisymmetric cases usually require the use of the TERPSICHORE code within the optimization for these global modes. In any case, with independence of the underlying symmetry, a careful post-optimization analysis of the final optimized configuration is required to confirm the accuracy of its stability properties. This is usually done using TERPSICHORE, which can carry out a very complete range of stability calculations, including global and local analysis, low- n and high- n pressure-driven and current-driven modes and fixed- and free-boundary calculations. But TERPSICHORE's performance can also be affected by the accuracy of the Boozer reconstruction (in addition to the accuracy of the VMEC equilibrium solution), which seems to be critical at low aspect ratios as indicated by the appearance of unphysical (or numerical) unstable modes in some of the NCSX configurations. A method for avoiding these modes has been implemented and is described in Section 4.

The complementary roles that COBRA and TERPSICHORE play within the compact stellarator design process thus makes the consistency of their results not only reassuring but essential. Clarifying such a comparison is the main purpose of this paper, and it is carried out in Section 5 using two compact de-

signs obtained from this optimization effort: the quasi-axisymmetric C82 configuration of the NCSX project at Princeton [7] and a high- τ case of the QOS project at Oak Ridge [4]. The comparison is by no means trivial since both codes address the high- n stability calculations in different ways, using different normalizations and different underlying equilibrium solutions due to the intermediate mapping to Boozer coordinates required by TERPSICHORE. In addition, the computed eigenvalues are not equivalent, which has caused some confusion in the past when interpreting their results. But this paper will show that despite the vast differences in approaches used by these stellarator stability codes, the results from both of them can be reliably used to compute high- n stability properties of low aspect ratio stellarators. Finally, some conclusions will be presented in Section 6.

2. Modifications of the VMEC code

The VMEC code [17], which uses a conjugate gradient method to solve the MHD inverse equilibrium equations, has been redifferenced to improve the convergence at lower aspect ratios and as well as for equilibria with a wider range of rotational transform profiles. At lower aspect ratios, the enhanced toroidal coupling of modes requires finer angular meshes (more poloidal modes) than was feasible in earlier versions of VMEC. In VMEC, the “inverse” equilibrium equations are cast as second order equations (with radius as the independent variable) for the Fourier components of the cylindrical coordinates R and Z , and μ , the renormalization stream function [notice that this stream function is referred to as λ in Ref. [17], but we prefer to use μ to avoid confusion with the eigenvalues to be introduced later on]:

$$\begin{aligned} R(s, \theta, \phi) &= \sum_{mn} R_{mn}(s) \cos(m\theta - n\phi), \\ Z(s, \theta, \phi) &= \sum_{mn} Z_{mn}(s) \sin(m\theta - n\phi), \\ \mu(s, \theta, \phi) &= \sum_{mn} \mu_{mn}(s) \sin(m\theta - n\phi), \end{aligned} \quad (1)$$

where (s, θ, ϕ) is a set of magnetic coordinates in which ϕ coincides with the geometrical toroidal angle, s is a radial coordinate varying from 0 at the magnetic axis to 1 at the last closed magnetic surface (plasma

boundary), and θ is a poloidal angle determined to accelerate the convergence in m -space of the Fourier series in Eq. (1).

In previous versions of VMEC, μ was differenced radially (in s) on a mesh centered between R , Z nodes, which greatly improved the radial resolution. This could be done to second order accuracy (in $h_s \equiv 1/(N_s - 1)$, with N_s the number of magnetic surfaces in the computational grid), since no radial derivatives of μ appear in its determining equation, $\mathbf{J} \cdot \nabla_s = 0$. Near the magnetic axis, however, a type of numerical interchange instability occurred as the angular resolution was refined (i.e. as the maximum poloidal mode number increased). This behavior has prevented the temporal convergence of 3D solutions with large numbers of poloidal (m) and toroidal (n) modes (typically, $m \sim 6-8$ was the practical limitation). It has also produced convergence problems for equilibria with very low rotational transforms, where field lines must encircle the magnetic axis many times to adequately resolve a magnetic surface. The new differencing scheme computes the stream function on the same mesh as R and Z (although the output values of μ continue to be on the centered-grid for backwards compatibility), which leads to numerical stabilization of the origin interchange. To avoid first order errors (in h_s) near the plasma boundary resulting from the new representation of μ , the radial current J_s continues to be internally represented (in terms of μ) on the centered-grid. This maintains the good radial spatial resolution associated with the original half-grid representation for μ . As a result, computation of convergent solutions with substantially higher mode numbers is now possible in VMEC ($m < 20$), corresponding to much finer spatial resolution and significantly improved force balance in the final equilibrium state. It also results in convergence for equilibria with low values of rotational transform, which was difficult to obtain with the previous differencing scheme.

An additional improvement in the output from VMEC includes a recalculation (once the VMEC equilibrium has been obtained) of the magnetic force balance $\mathbf{F} = (\mathbf{J} \times \mathbf{B} - \nabla p) = 0$. The radial (∇_s) component of \mathbf{F} is solved in terms of the non-vanishing contravariant components of \mathbf{B} (B^θ and B^ϕ) and the metric elements determined by VMEC, as a magnetic differential equation for B_s . An angular collocation procedure (with grid points matched to the Nyquist spa-

tial frequency of the modes) is used to avoid aliasing arising from nonlinear mode coupling of Fourier harmonics of R and Z in the inverse representation of the equilibrium equation. The accurate determination of B_s , together with the improved angular resolution afforded by the larger limits on the allowable (m, n) spectra, permits an accurate assessment for the parallel current (which contains angular derivatives of B_s , as a function of poloidal mode number, to be performed. Studies of the Hamada condition, and its impact on Mercier stability, near low order rational surfaces and comparison with the PIES code are presently underway [8].

3. The COBRA ballooning code

The COBRA code can in principle solve the standard ideal ballooning equation [30] in any set of magnetic coordinates (s, θ, ϕ) :

$$\left[\frac{d}{d\phi} \left[P(\phi) \frac{d}{d\phi} \right] + Q(\phi) + \lambda R(\phi) \right] F(\phi) = 0 \quad (2)$$

with $P = B^\phi |\mathbf{k}_\perp|^2 / B^2$, $R = P / (B^\phi)^2$ and $Q = \epsilon^2 \beta_0 p' \kappa_s / B^\phi$. The field line curvature is given by $\bar{\kappa}$, the pressure gradient is p' and $\epsilon = a / R_0$ is the inverse aspect ratio (a is the minor radius and R_0 the major radius). Magnetic fields are normalized to B_0 , parallel and perpendicular lengths respectively to R_0 and a and times to the Alfvén time. $\beta_0 \equiv 2\mu_0 p_0 / B_0^2$, with p_0 the axis pressure. In contrast to TERPSICHORE (see Section 4), COBRA uses the toroidal angle ϕ to parametrize the field line (instead of the poloidal angle). The first term on the left-hand side of Eq. (2) corresponds to the stabilizing influence of the bending of magnetic field lines, the last one is the stabilizing contribution of inertia, while the Q -term, proportional to the pressure gradient, drives the instability in those regions with bad curvature when the pressure gradient exceeds some threshold. This threshold is responsible for the β stability limit due to ballooning modes. $P(\phi)$ is written in a way that it satisfies positiveness in all cases, independently of the accuracy of the VMEC solution, to avoid the appearance of unphysical modes (see Section 4).

Integrability of the eigensolution F along the field line determines the eigenvalue, λ , that is related to the ballooning growth rate, γ , normalized to the inverse

Alfvén time, by $\lambda = -\gamma^2$. COBRA solves Eq. (2) on any set of magnetic surfaces of the configuration, on any set of initial locations on those surfaces and for any set of values of the arbitrary ϕ_k parameter (similar to the θ_k parameter in TERPSICHORE), whose secular dependence is imbedded in both $\bar{\mathbf{k}}_\perp$ and κ_s .

COBRA computes λ very quickly by taking advantage of the Sturm–Liouville character of Eq. (2). This property allows an estimate for the eigenvalue to 4th-order accuracy (in the mesh step size along the magnetic field line) by variationally refining a previous 2nd-order accurate estimation of the eigensolution, F , obtained by standard matrix methods:

$$\lambda = - \frac{\langle F, LF \rangle}{\langle F, RF \rangle}, \quad (3)$$

where the following definitions have been used for the differential operator L and the inner product $\langle \cdot, \cdot \rangle$ in $L^2(-\infty, +\infty)$:

$$L(\phi) \equiv \frac{d}{d\phi} \left[P(\phi) \frac{d}{d\phi} \right] + Q(\phi), \quad (4)$$

$$\langle F, G \rangle \equiv \int_{-\infty}^{+\infty} G^*(\phi) F(\phi) d\phi$$

and with P , R and Q being the functions appearing in Eq. (2). The size of the numerical integration box is set by choosing how many “helical wells” along the magnetic field line are included in the calculation. Each helical well approximately corresponds to a toroidal displacement of the order of $2\pi/M$, with M the periodicity of the configuration. The number of “helical wells”, K_w , to be used will depend on the degree of localization of the eigenmode along the field line (see Section 5 for some examples).

A fast and accurate evaluation of the eigenvalue is then achieved by coupling this evaluation process to a Richardson’s extrapolation scheme, that will extrapolate, using a quartic function, to zero mesh-step size from a few previous eigenvalue evaluations on very coarse (and therefore rapidly evaluated) meshes. For comparison, TERPSICHORE integrates a similar equation (see Section 4) using a fixed-step shooting algorithm. Accuracy is then a function of the number of mesh points used, which makes it a relatively more time-consuming calculation.

The original version of COBRA was based on straight magnetic (Boozer) coordinates. It was re-

cently modified to carry out calculations directly in VMEC coordinates to further enhance computational efficiency and to prevent convergence and accuracy problems common to ALL codes based on Boozer coordinates. In this version, the magnetic field line must be followed numerically at the same time that Eq. (2) is solved in a way that does not interfere with the efficiency of the Richardson's scheme. Use is made of the fact that any magnetic line on any given magnetic surface, labeled by s , satisfies an equation of the type:

$$\theta - \tau\phi + \mu(s, \theta, \phi) = \alpha \quad (5)$$

for some constant value α , that is used as line label, and with the stream function μ provided by the VMEC code (see Section 2). Therefore, θ can be obtained along the magnetic line by solving the following equation for $\theta(\phi)$:

$$G(\theta) \equiv \theta - \tau\phi + \mu(s, \theta, \phi) - \alpha = 0 \quad (6)$$

using a Newton–Raphson scheme that iterates:

$$\theta^{k+1} = \theta^k - \frac{G(\theta^k)}{dG(\theta^k)/d\theta}. \quad (7)$$

The overall speed has in this way been increased more than a hundred times relative to most standard codes. [Many more details about the solution scheme here sketched and its mathematical and numerical basis can be found in Refs. [15,16] and references there.]

4. Modifications of the TERPSICHORE code

The ideal MHD stability code TERPSICHORE [19] was developed in the late 80s and early 90s. It has been routinely used for the numerical assessment of global and local stability properties of many stellarators (for instance, the ATF stellarator at Oak Ridge National Laboratory [23], the W-7X advanced helias currently under construction in Germany [24] or the HSX quasi-helical stellarator recently built at the University of Wisconsin [25]). TERPSICHORE's performance regarding ideal global stability has also been benchmarked against the well-known CAS3D stability code [20] for several large aspect ratio configurations [26].

TERPSICHORE (as almost all MHD stability codes) carries out all its computations in Boozer coordinates [18], (s, θ_b, ϕ_b) , since magnetic field lines are

then simply defined as $\theta_b - \tau\phi_b = \alpha$, for some real number α , and the magnetic field vector has very simple representations:

$$\begin{aligned} B_i &= (B_s, J, -I), \\ \sqrt{g}B^i &= (0, \Psi', \Phi'). \end{aligned} \quad (8)$$

This considerably simplifies analytic manipulations (Ψ and Φ are the toroidal and poloidal magnetic fluxes, J and I the toroidal and poloidal current fluxes and \sqrt{g} is the Jacobian of the coordinate transformation). Instead of just mapping the VMEC equilibrium to these coordinates, TERPSICHORE carries out a recalculation from the VMEC solution to guarantee that the plasma current satisfies $\nabla \cdot \mathbf{J} = 0$ also at rational surfaces. This causes the parallel current to diverge, which is missed by the VMEC solution (even when this has been somewhat relieved by the changes described in Section 2), causing the typical spikes appearing at rational surfaces in the Mercier criterion for interchange instability [24].

To estimate high- n ballooning stability, TERPSICHORE solves for the eigenvalue of a modified Euler–Lagrange equation derived from the MHD energy principle. When expressed in Boozer coordinates, it takes the form [28]:

$$\frac{d}{d\theta_b} \left(C_b \frac{dF}{d\theta_b} \right) + (1 - \lambda)C_a F = 0, \quad (9)$$

where F determines the eigenvalue λ when forced to be an integrable function along the field line. The C_b term, related to the stabilizing energy associated with bending of magnetic field lines, is proportional to $\mathbf{k}_\perp^2 / (\sqrt{g}B^2)$ with $\mathbf{k}_\perp = \nabla(\phi_b - q\theta_b) + q'\theta_k \nabla s$, and is strictly positive. Here, q is the inverse of the rotational transform and θ_k is an arbitrary parameter related to the radial mode number. Finally, $C_a = d_p + d_s(\theta_b - \theta_k)$ is the destabilizing term, proportional to the pressure gradient and the local magnetic curvature (the exact expression for d_p and d_s can be found in Ref. [24]). λ is not the growth rate of the mode (the mode inertia, proportional to the squared growth rate, is not included when the energy principle is minimized in this fashion) but when it is positive, the mode is unstable.

Regarding the numerical method used to integrate Eq. (9), TERPSICHORE uses a 2nd-order accurate shooting method. It integrates the solution from the

two end points of the integration box towards the center, being the eigenvalue λ determined by requiring the first derivative of the solution to be continuous at the middle point. The size of the integration box is set by the number of poloidal circuits along the field line: the poloidal angle is varied from $-2\pi S_0$ to $+2\pi S_0$, with S_0 the number of transits. Convergence of the eigenvalue therefore requires a sufficiently large value of S_0 (depending on the degree of localization of the mode) and a sufficiently dense mesh along the line.

The appearance of unphysical ballooning modes in the NCSX cases is related to the line bending term, which can be written explicitly as follows:

$$C_b = C_p + C_s(\theta_b - \theta_k) + C_q(\theta_b - \theta_k)^2 \quad (10)$$

with:

$$\begin{aligned} C_p &= \frac{g_{ss}}{\sqrt{g}} - \frac{B_s^2}{B^2\sqrt{g}}, \\ C_s &= \frac{2q'\Psi'}{\Phi'} \left(\frac{JB_s}{B^2\sqrt{g}} - \frac{g_s\theta_b}{\sqrt{g}} \right), \\ C_q &= \frac{q'^2\Psi'^2|\nabla s|^2}{B^2\sqrt{g}}. \end{aligned} \quad (11)$$

Analytically, C_b is strictly positive. However, it can become (numerically) negative at some locations along the magnetic field line if the VMEC equilibrium solution and/or the Boozer reconstruction are not sufficiently accurate. Numerical simulations seem to suggest that this happens more frequently at lower aspect ratios, most likely due to the larger number of modes required both in the equilibrium solution as well as in the Boozer transformation. When this is the case, the potential in the Schrödinger equation obtained from Eq. (9) by a variable transformation [29] exhibits infinite barriers at the locations where $C_b = 0$. These are capable of trapping an unphysical unstable mode. To prevent these unphysical solutions, the line bending term in TERPSICHORE has been rewritten using a representation that ensures positiveness independently of the equilibrium accuracy [21]:

$$C_b = C_1(1 + [C_2 + C_3(\theta_b - \theta_k)]^2), \quad (12)$$

with

$$C_1 = \frac{1}{\sqrt{g}|\nabla s|^2},$$

$$C_2 = \frac{-I g_s \theta_b}{B\sqrt{g}} + \frac{J g_s \phi_b}{B\sqrt{g}}, \quad (13)$$

$$C_3 = \frac{q'\Psi'|\nabla s|^2}{B},$$

where several relationships between the Boozer metric coefficients and magnetic fluxes have been used. It is straightforward to relate the new C_i with the old coefficients:

$$\begin{aligned} C_q &= C_1 C_3^2, \\ C_s &= 2C_1 C_2 C_3, \\ C_p &= C_1(1 + C_2^2). \end{aligned} \quad (14)$$

5. COBRA-TERPSICHORE benchmarking

Ideal MHD pressure-driven instabilities comprise both interchange and ballooning modes [31]. They both satisfy $k_\perp \gg k_\parallel$, being therefore amenable of a local analysis when represented by means of the ballooning formalism [32]. Using this representation, stability β -limits against both interchange and ballooning modes can be studied by solving an ordinary differential equation (Eqs. (2) or (4)) along the magnetic field line. The properties of the resulting eigensolution is however very different for interchanges and ballooning modes. Interchanges extend along the magnetic field line for many helical magnetic wells (strictly speaking, they are only defined in the limit $k_\parallel \rightarrow 0$, but here, any solution of the ballooning equation satisfying $k_\parallel R_0 \ll 1$ will be referred to as an interchange). As a result of this extended structure, they are usually found linked to the lower-order rational surfaces of the configuration. In contrast, ballooning modes are typically highly localized ($k_\parallel R_0 \gg 1$) [15,33], extending for only a few helical wells.

Taking advantage of their large extension along the field lines, an asymptotic analysis can be used to derive a stability criterion for interchanges (see, for instance, Ref. [28]), completely analogous to that originally derived by Mercier [27]. From this analysis, it is clear that interchange modes are destabilized on a magnetic surface if the surface-average of the line-curvature and parallel currents is large enough as to oppose the stabilizing effect of the surface-averaged magnetic well or shear. Since the evaluation

of this criterion only involves the computation of these few surface-averaged quantities, it is the usual method to determine the stability β -limits of the configurations against interchange modes, and it is thus routinely included in the compact stellarator optimization loop (in fact, it has been included in the latest release of VMEC). This asymptotic method is much faster than trying to evaluate their exact growth rates by solving Eqs. (2) or (4), since it is then necessary to include in the numerical box along the field line a very large number of helical wells K_w in COBRA (see Section 3) or poloidal transits S_0 in TERPSICHORE (see Section 4). This fact, together with the requirement of keeping a sufficiently dense mesh of points along the line to get a well-converged eigenvalue, turns the computation very slow.

On the other hand, localized ballooning modes are rather insensitive to any of the aforementioned surface-averaged quantities, being however driven or damped by the local magnetic shear, local current densities and local curvatures. This implies that: (1) a detailed knowledge of these local quantities is necessary to estimate their growth rates, which implies that the equilibrium solution must be locally accurate and with good local force balance to yield reliable results and (2) no ballooning version of the Mercier criterion exists. The fast ballooning growth rate estimation that COBRA produces is the closest to such a criterion we have been able to achieve for localized ballooning modes. Since the growth rate can be obtained at several locations and several surfaces very quickly, COBRA can be used to generate a positive target function (for instance, by using the sum of all positive growth rates) whose minimization would eventually increase the critical β above which the configuration becomes unstable to ballooning modes [34].

From this discussion, it seems obvious that, in the context of ideal pressure-driven instabilities, there are two essential results that need to be benchmarked between COBRA and TERPSICHORE: (1) agreement on the determination of the regions of the configuration where unstable interchange (also referred to as extended-ballooning modes throughout the paper) appear for any prescribed value of $\langle\beta\rangle$ (noticing that these regions should coincide with those surfaces where the equilibrium violates the Mercier criterion for stability) and (2) agreement on the determination of the regions of the configuration where

localized-ballooning modes turn unstable for any $\langle\beta\rangle$ (notice that these regions may now as well be Mercier stable as Mercier unstable; if Mercier unstable, this would mean that more than one unstable eigenvalue exists in the discrete spectrum of Eqs. (2) or (4); the most unstable one would correspond to the localized mode and the others, to more extended interchange-like modes).

But before beginning the benchmarking process, it will prove useful to point out now the differences between the eigenvalues λ calculated by COBRA and TERPSICHORE: Eq. (9) is recovered from Eq. (2) (apart from normalization issues) if the inertial term R is set to zero and if the destabilizing Q -term is multiplied by $(1 - \lambda)$. Therefore, both equations are only identical in the limit $\lambda \rightarrow 0$, i.e. for marginal stability. This implies that COBRA and TERPSICHORE will predict the same instability regions and the same thresholds for β , but the user should not expect the same eigenvalues for any unstable surface. TERPSICHORE will yield a positive λ , while COBRA will yield a positive growth rate and thus a negative λ . More unstable surfaces will yield larger positive λ 's in TERPSICHORE and smaller (more negative) λ 's in COBRA, corresponding to larger positive growth rates. On top of this, we should also keep in mind that COBRA uses the VMEC equilibrium solution while TERPSICHORE uses its own Boozer reconstruction, which implies that the two equilibria are not identical (for instance, they will specially differ at rational surfaces, where $\nabla \cdot \mathbf{J}$ is small but nonzero for the VMEC solution. This was already made apparent when comparing the results obtained from evaluating the Mercier criterion directly in VMEC coordinates and in Boozer coordinates for the W7-X stellarator in Ref. [24]). At the same time, extra inaccuracies are present in the equilibrium reconstruction carried out by TERPSICHORE, whose relative importance will strongly depend of the number of Boozer modes included. Finally, it is good to keep in mind that to use numerical boxes of the same length in both codes, the number of poloidal transits in TERPSICHORE must be set to $S_0 \sim K_w \tau / M$, with K_w the number helical wells used in COBRA.

We will then begin by benchmarking the first point by choosing a compact stellarator case where interchange-like modes exist above some critical value of β , but no localized-ballooning mode is found. This

state of things can be ensured by choosing a configuration where the Mercier criterion predicts instability but no unstable solution is found when solving the ballooning equation until the numerical box exceeds a minimum length. As an example of such a case we use C82, a previous reference configuration of the NCSX project [8]. This is a $M = 3$ quasi-axisymmetric equilibrium with aspect ratio $A \sim 3.4$, magnetic field $B \sim 2T$ and almost 50% of the rotational transform, τ , provided by the bootstrap current. Its rotational transform increases monotonically from 0.26 at the axis to 0.47 at the edge at $\beta = 3\%$. The numerical equilibria for this case have been computed for values of $\langle\beta\rangle$ ranging from 3 to 5% using 97 radial points, and with 8 poloidal and 5 toroidal VMEC modes (83 modes in total), keeping the total toroidal current profile fixed, and letting τ be modified by the increasing β . The reason for this choice, is that it will help to identify the interchange character of the unstable modes, since they tend to be located near rational surfaces and will therefore try to follow them as the τ profile is modified. The most unstable modes are usually found at the locations with the most unfavorable curvature that, in this configuration, is found around $(\theta, \zeta) = (0, 0)$ and its periods and semiperiods. Therefore, the ballooning equation has been solved for eigensolutions centered at this location.

We have used COBRA to build a map of the unstable regions in β - s space (remember that s is the magnetic surface label, that in VMEC corresponds to the toroidal magnetic flux). This map is shown in Fig. 1, with the shaded regions corresponding to those regions where unstable solutions are found. The interchange character of the unstable modes is readily confirmed by the close alignment of the unstable regions with the lower-order rationals present in the configuration: $\tau = 3/7, 3/8, 3/9, 3/10$ and $3/11$. TERPSICHORE can be seen to reproduce the same instability regions for all values of $\langle\beta\rangle$. As an example, dark solid lines have been superimposed to the map, corresponding to the radial regions where TERPSICHORE finds unstable solutions for the equilibria with $\langle\beta\rangle = 3.25, 3.85$ and 4.25% . A more detailed comparison is carried out for the equilibrium with $\langle\beta\rangle = 3.85\%$ in Fig. 2. The eigenvalue λ obtained by TERPSICHORE and the growth rate $\gamma = -\lambda^2$ obtained by COBRA are there shown as a function of the toroidal flux. The gray-

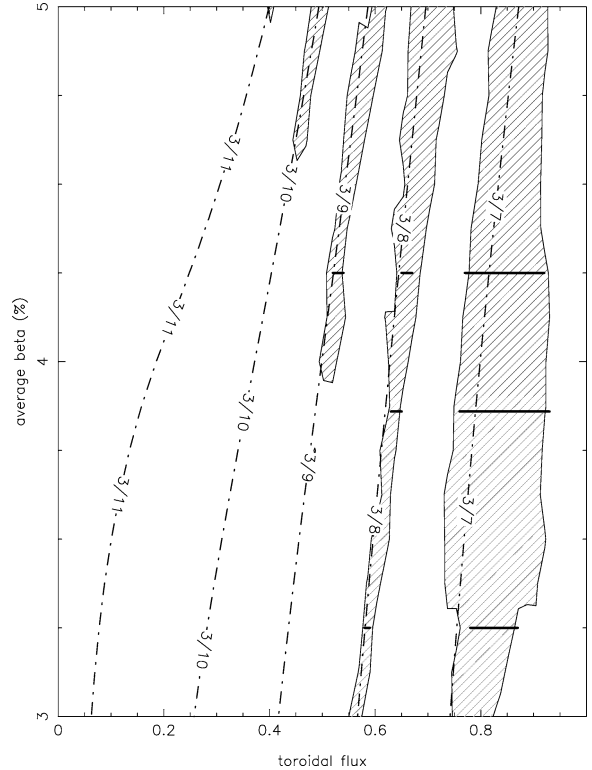


Fig. 1. Contour map in $\langle\beta\rangle$ - s space of the growth-rates obtained by COBRA for the QAS configuration C82. The unstable regions are shaded in gray. Thick solid lines show the regions where unstable modes are found by TERPSICHORE for a subset of selected equilibria. The radial location of the lower-order rational surfaces is also shown using dot-dashed lines.

shaded regions correspond now to those radial locations where the Mercier criterion predicts interchange instability for that equilibrium. Both codes can be seen to detect these unstable extended modes in very good agreement with the Mercier criterion. The good convergence of the growth-rates is also shown in Fig. 3, using a contour map in K_w - s space of the growth rates obtained by COBRA for the same equilibrium. Notice that a growth rate obtained at any arbitrary magnetic surface would be well converged only for a number of wells above which, the contour passing through that surface becomes a straight vertical line (this would imply that the same growth rate would be obtained for any larger box!). Notice that, for this equilibrium, this is not the case until $K_w \sim 65$, which corresponds to using $S_0 \sim 10$ – 12 poloidal transits in TERPSICHORE. The growth rates and eigenvalues in-

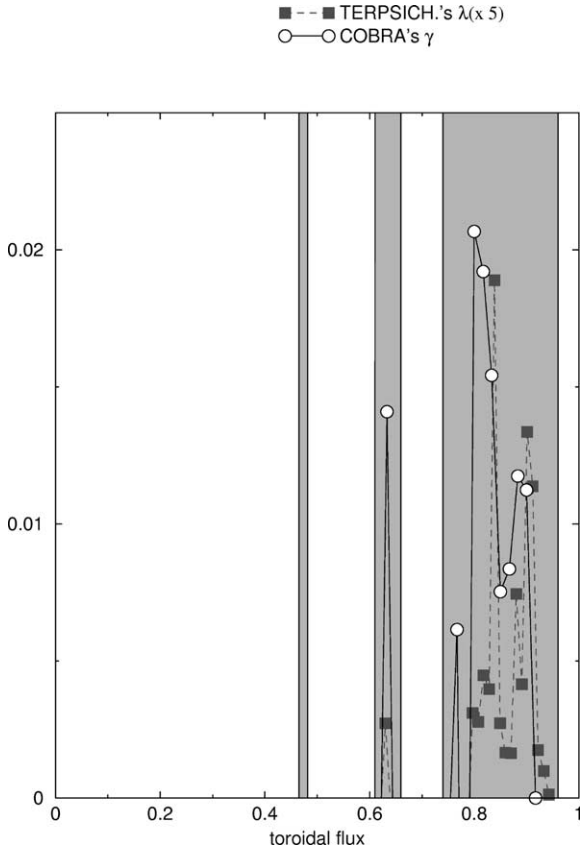


Fig. 2. Comparison of the eigenvalue λ obtained by TERPSICHORE and the growth rate γ computed by COBRA for the C82 equilibrium with $\langle\beta\rangle = 3.85\%$. Mercier unstable regions are shaded in gray.

cluded in Fig. 2 have therefore been computed using respectively $K_w = 70$ and $S_0 = 12$. The good convergence of the TERPSICHORE results have also been ensured independently by rerunning on all surfaces with a higher value of S_0 . As a final comment, the contour map in Fig. 3 confirms again the interchange-like character of the modes: it can be appreciated that no unstable mode is located if $K_w < 20$ is used!

In order to compare now COBRA and TERPSICHORE when detecting localized-ballooning modes, we have turned to a high- ι compact quasi-omnigenous (QOS) case that has been altered on purpose to reduce its ballooning stability β -limits. This QOS case has also three periods ($M = 3$), aspect ratio $A \sim 3.5$, $B \sim 1T$ and a small total bootstrap current ($I_p < 50kA$ for $\langle\beta\rangle = 3\%$). Its rotational transform ι steadily increases from an axis value of 0.55 to close to 0.65 at

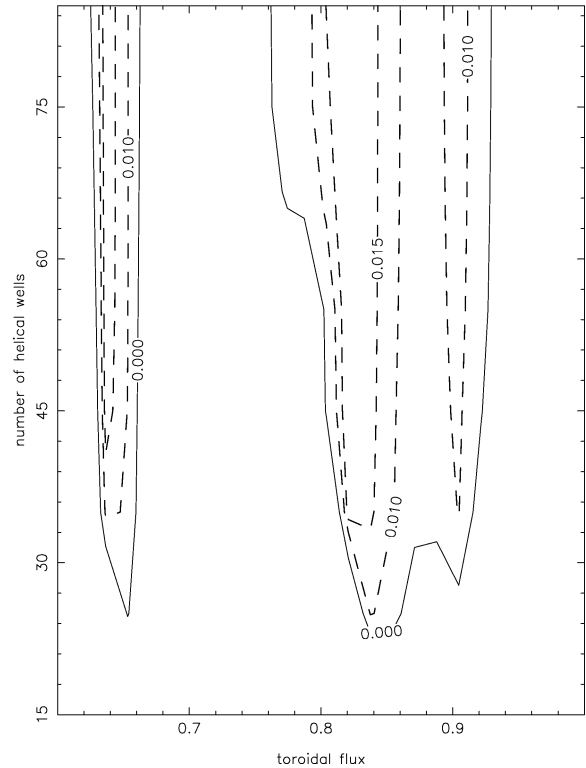


Fig. 3. Contour map in K_w - s space of the growth rates obtained by COBRA for the c82 equilibrium with $\langle\beta\rangle = 3.85\%$.

the plasma edge [4]. We have computed a series of equilibria with values of $\langle\beta\rangle$ ranging from 0 to 3%. A fixed ι profile has now been chosen, and 97 radial surfaces, 8 VMEC poloidal modes and 5 VMEC toroidal modes have been used. Analogously to what we did in the NCSX case, we build a contour map in $\langle\beta\rangle$ - s space of the most unstable growth rate obtained by COBRA, which is shown in Fig. 4. Again, the shaded areas correspond to unstable solutions. The comparison with TERPSICHORE is done in the same way as before: the dark solid lines correspond to the regions where unstable solutions are found by TERPSICHORE for those equilibria with $\langle\beta\rangle = 1, 2, 2.5$ and 3%. The agreement with COBRA is again remarkable. A more detailed comparison for the equilibrium with $\langle\beta\rangle = 3\%$ is also shown in Fig. 5, with the gray-shaded regions again representing those locations where the Mercier criterion for stability is violated. It can now be appreciated that all modes encountered outside these gray-shaded regions are truly localized

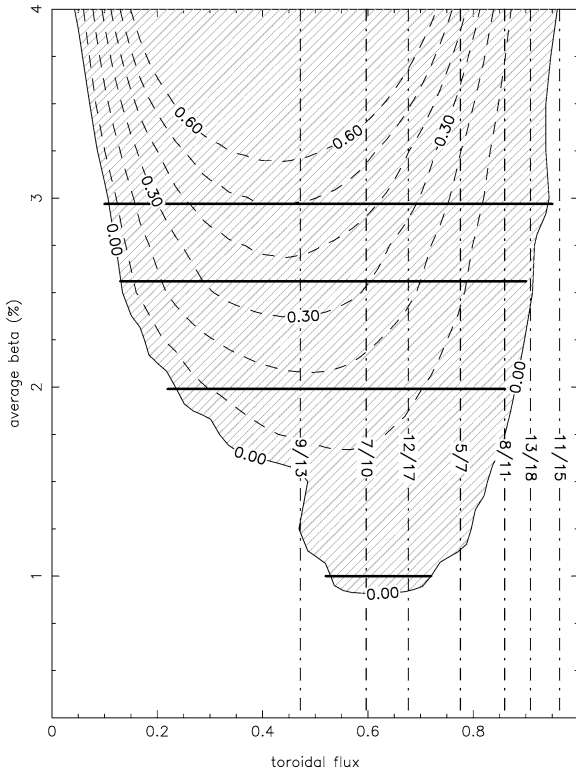


Fig. 4. Contour map in (β) - s space of the growth-rates obtained by COBRA for the QOS configuration. The unstable regions are shaded in gray. Thick solid lines show the regions where unstable modes are found by TERPSICHORE for a subset of selected equilibria. The radial location of the lower-order rational surfaces is also shown using dot-dashed lines.

solutions by looking at the growth-rate contour map in K_w - s space for this equilibrium: the growth rate is well converged in the Mercier-stable region even for $K_w < 5$ all throughout that region (as a matter of fact they can be obtained even if setting $K_w = 2$!). In the Mercier-unstable shaded region, highly-localized modes still exist until $s \sim 0.75$, indicating the coexistence of a less unstable extended mode, that is readily revealed when looking for the second most unstable mode with COBRA. For $s > 0.75$, the most unstable mode becomes now an extended-ballooning mode, requiring at least $K_w \sim 30$ helical wells for its growth rate to converge at $s = 0.95$. To ensure convergence of growth rates and eigenvalues included in Fig. 5 for ALL surfaces, they have been computed respectively using $K_w = 40$ and $S_0 = 12$ in COBRA and TERPSICHORE.

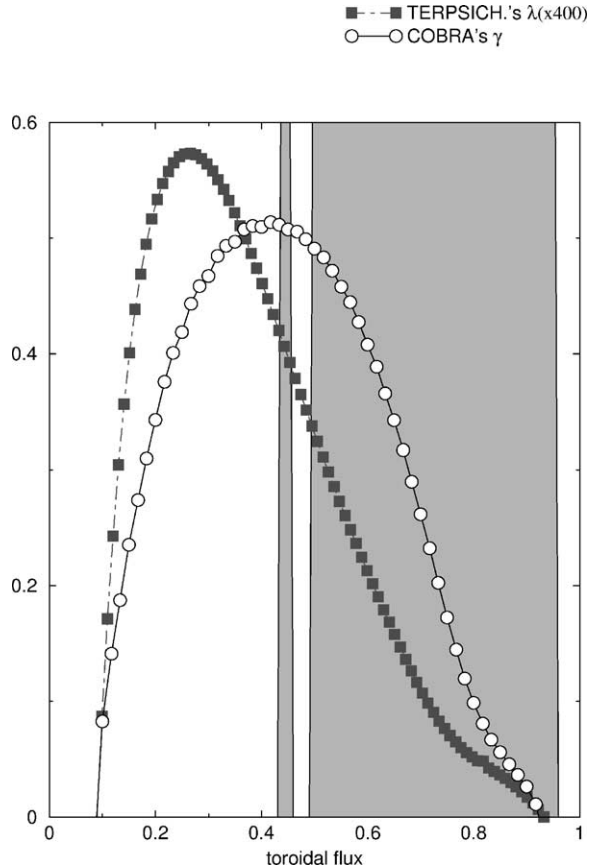


Fig. 5. Comparison of the eigenvalue λ obtained by TERPSICHORE and the growth rate γ computed by COBRA for the QOS equilibrium with $\langle \beta \rangle = 3\%$. Mercier unstable regions are shaded in gray.

6. Conclusions

It is difficult to carry out a benchmarking between codes that, even when addressing in principle the same problem (local pressure-driven modes), use different solution techniques, as it is the case for COBRA and TERPSICHORE. They use different normalizations, slightly different forms of the MHD equilibria, different coordinates and even compute different eigenvalues from different equations. In spite of these differences, it is reassuring to have shown that both COBRA and TERPSICHORE predict the same regions of interchange and ballooning instability, and similar critical β , for the low aspect ratio stellarators we have investigated in this paper. This successful benchmarking ensures that ideal stability calculations are reliable

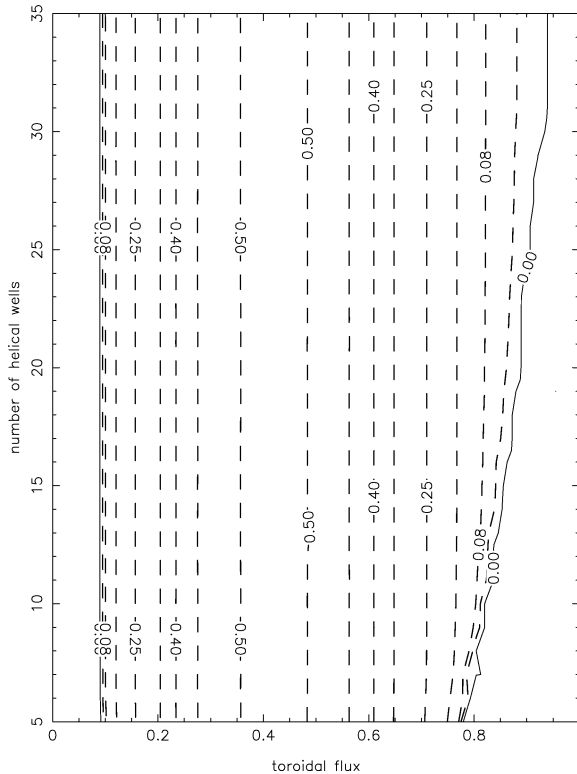


Fig. 6. Contour map in K_w - s space of the growth rates obtained by COBRA for the QOS equilibrium with $\langle\beta\rangle = 3\%$.

in the complex optimization process that need to be undertaken to find attractive low-A stellarator configurations.

Acknowledgements

This work was sponsored by Spanish DGES project FTN2000-0924-C03-01, the U.S. Department of Energy under contracts DE-AC02-76CH03073 and DE-AC05-00OR22725, EURATOM and the Fonds National Suisse pour la Recherche Scientifique. Russian authors are grateful to Prof. J. Nührenberg for providing us with access to a NEC-SX5 supercomputer (RZG, IPP, FRG). This work was made in the frame of CRPP-IPM collaboration and also supported by IN-MARCON (Moscow, Russia).

References

- [1] L. Spitzer Jr., U.S. Atomic Energy Commission Report No. NYO-993 (PM-S-1), 1951; U.S. Atomic Energy Commission Report No. NYO-995 (PM-S-3), 1951.
- [2] J. Nührenberg, R. Zille, Phys. Lett. A 129 (1988) 113.
- [3] J. Nührenberg, W. Lotz, P. Merkel et al., Trans. Fusion Technology 27 (1995) 71.
- [4] S.P. Hirshman et al., Phys. Plasmas 6 (1999) 1858.
- [5] C. Beidler et al., Fus. Technol. 17 (1961) 149.
- [6] A. Iiyoshi, M. Fujiwara, O. Motojima, N. Ohyaib, K. Yamazaki, Fus. Technol. 17 (1990) 169.
- [7] G.H. Neilson et al., Phys. Plasmas 7 (2000) 1911.
- [8] A.H. Reiman et al., Phys. Plasmas 8 (2001) 2083.
- [9] S. Okamura et al., in: Proc. 18th IAEA Conference on Fusion Energy, Sorrento, Italy, 2000.
- [10] J.R. Cary, S.G. Shasharina, Phys. Rev. Lett. 78 (1997) 674.
- [11] S.P. Hirshman et al., Phys. Rev. Lett. 80 (1998) 528.
- [12] D.A. Spong et al., Nucl. Fusion 41 (2001) 711.
- [13] J.M. Greene, J.L. Johnson, Phys. Fluids 4 (1961) 871.
- [14] L. García, B.A. Carreras, N. Domínguez, J.N. Leboeuf, V.E. Lynch, Phys. Fluids B 2 (1990) 2162.
- [15] R. Sánchez, S.P. Hirshman, J.C. Whitson, A.S. Ware, J. Comput. Phys. 161 (2000) 576.
- [16] R. Sánchez, S.P. Hirshman, H.V. Wong, Comput. Phys. Comm. 135 (2001) 82.
- [17] S.P. Hirshman, W.I. van Rij, P. Merkel, Comput. Phys. Comm. 43 (1986) 143.
- [18] A.H. Boozer, Phys. Fluids 23 (1980) 904.
- [19] D.V. Anderson, W.A. Cooper, R. Gruber, S. Merazzi, U. Schwenn, J. SuperComput. Appl. 4 (1990) 34.
- [20] C. Schwab, Phys. Fluids 5 (1993) 3195.
- [21] J. Nührenberg, R. Zille, in: Theory of Fusion Plasmas, Proc. of the 1987 Varenna Workshop, Editrice Compositori, Bologna, 1986, p. 3.
- [22] G.Y. Fu et al., Phys. Plasmas 7 (2000) 1809.
- [23] W.A. Cooper, S.P. Hirshman, D.K. Lee, Nucl. Fusion 29 (1989) 617.
- [24] R. Moeckli, W.A. Cooper, Nucl. Fusion 33 (1993) 1899.
- [25] J. Talmadge, W.A. Cooper, Phys. of Plasmas 3 (1996) 3713.
- [26] J. Nührenberg et al., Plasm. Phys. Contr. Fus. 35 (1993) B115.
- [27] C. Mercier, Nucl. Fusion 1 (1960) 47.
- [28] W.A. Cooper, Plasm. Phys. Contr. Fus. 34 (1992) 1011.
- [29] P.M. Morse, H. Feshbach, Methods for Theoretical Physics, McGraw-Hill, New York, 1953.
- [30] D. Correa-Restrepo, Zeit. Naturf. 37 (1982) 848.
- [31] J.P. Freidberg, Rev. Mod. Phys. 54 (1982) 801.
- [32] J.W. Connor, R.J. Hastie, J.B. Taylor, Proc. Roy. Soc. London A 365 (1979) 1.
- [33] N. Nakajima, Phys. Plasmas 3 (1996) 4556.
- [34] R. Sánchez, S.P. Hirshman, A.S. Ware, L.A. Berry, D.A. Spong, Plasm. Phys. Contr. Fusion 42 (2000) 641.